J. Mater. Environ. Sci. 7 (9) (2016) 3387-3398
ISSN : 2028-2508
CODEN: JMESC

Silybum Marianum oil as green inhibitor for carbon steel corrosion in 1 M HCl solution: Electrochemical and SEM investigations

S. Alaoui Ismaili[1], H. Bourazmi[2], H. Harhar[3]*, M. Tabyaoui[2], A. Guenbour[2], A. Bellaouchou[2], M. EL Moudane[2], A. Zarrouk[5], S. Kitane[4], M. Alaoui El Belghiti[1]

1 Laboratoire de Chimie Physique Générale, Département de Chimie, Université Mohammed V, Faculté des Sciences, Avenue Ibn Batouta, BP 1014. Morocco.

2 Laboratory of Materials, Nanotechnology and Environment, Faculté des Sciences, Université Mohammed V, BP 1014- Rabat, Morocco.

3 Laboratoire de Chimie des Plantes et de Synthèse Organique et Bioorganique, Faculté des Sciences, Université Mohammed V, BP 1014- Rabat, Morocco.

4 Laboratoires de chimie appliquée à l'Ecole Nationale de l'Industrie Minérale, Avenue Hadj Ahmed Cherkaoui BP 753 Agdal Rabat, Morocco

5 LCAE-URAC 18, Faculty of Science, First Mohammed University, PO Box 717, 60 000 Oujda, Morocco.

Received 29 May 2016, Revised 24 Aug 2016, Accepted 02 Sep 2016
**Corresponding author. E-mail: hichamoo79@yahoo.fr; Phone: ++212 668799942*

Abstract

Silybum Marianum oil (SMO) was tested as corrosion inhibitor for carbon steel in 1 M HCl using potentiodynamic polarization (PDP), electrochemical impedance spectroscopy (EIS) and scanning electron microscope (SEM). The effect of temperature on the corrosion behavior of carbon steel in 1 M HCl with addition of SMO was studied in the temperature range of 303-333 K. The experimental results reveal that SMO has a good inhibiting effect on the metal tested in 1 M HCl solution. Potentiodynamic polarization (PDP) studies clearly reveal that it acts essentially as a mixed mode of action. The protection efficiency increases with increasing of inhibitor concentration to attain 89.1 % at 3g L^{-1}. EIS results show that the charge transfer resistance R_{ct} increases with increasing of SMO concentration. The change in the impedance parameters (R_{ct} and C_{dl}) with concentration of SMO is indicative of the adsorption of molecules leading to the formation of a protective layer on the surface of carbon steel. SEM analysis substantiated the formation of protective layer over the carbon steel surface. It is evident from the results of this study that SMO inhibits the corrosion in 1M HCl through adsorption process following the Temkin adsorption isotherm. The thermodynamic data of activation are determined and discussed.

Keywords: Carbon steel, HCl, Corrosion inhibition, *Silybum Marianum* oil, Electrochemichal techniques, SEM.

1. Introduction

Corrosion protection is an important issue for industrial application of materials. Acid solutions are generally used for the removal of undesirable scale [1-3]. Hydrochloric and sulphuric acid are widely used in the pickling processes of metals resulting in huge economic losses [4-10]. Several researchers studied the effect of some organic inhibitors compounds containing heteroatoms are commonly used to reduce the corrosion attack on steel in acid solutions, those that are non-toxic or low-toxic to both human beings and environment. The use of non-toxic inhibitors called green or eco-friendly environmental inhibitors is one of the solutions possible to prevent the corrosion of the material [11-13]. Our laboratory draw a large part of program to examine natural substances

as corrosion inhibitors such as: *Euphorbia falcata* extract [11], *Artemisia Mesatlantica* essential oil [13], Argan oil [12]. All of which have been reported to be good inhibitors for metals and alloys in acidic solutions. Accordingly, the aim of this work is to study the inhibition action of *Silybum Marianum* oil (SMO), on the corrosion of carbon steel in hydrochloric acid. The inhibition performance is evaluated by electrochemical impedance spectroscopy (EIS) and potentiodynamic polarization measurements, complemented with scanning electron microscopy.

2. Experimental

2.1. Plant material

The Silybum Marianum was collected from the area of Rabat (Morocco) in April 2015; the dried plant material was stored in the laboratory at room temperature (298 K) and in the shade before the extraction.

2.2. Oil extraction

Oil extraction and yield quantification: Twenty g of ground kernels were extracted in a Soxhlet apparatus with 150 mL of boiling n-hexane for 8 h. The organic phase was collected, concentrated under vacuum, and dried for 5 min at 105°C. Extraction yield was determined using the official recommendation [14], and the oil was used for the analyses.

2.3. Fatty acid composition

FA was determined using method ISO 5508 [15]. Before analysis, fatty acids (FAs) were converted to fatty acid methyl esters (FAMEs) by shaking a solution of 60 mg oil and 3 mL of hexane with 0.3 mL of 2N methanolic potassium hydroxide. FAs were analyzed by gas chromatography using a Varian CP-3800 (Varian Inc.) chromatograph equipped with a FID. The column used was a CP-Wax 52CB column (30 m×0.25 mm i.d.; Varian Inc., Middelburg, The Netherlands). The carrier gas was helium and the total gas flow rate was 1 mL/min. The initial and final column temperature was 170 °C and 230 °C, respectively, and the temperature was increased by steps of 4°C/min. The injector and detector temperature was 230°C. Data were processed using a Varian Star Workstation v 6.30 (Varian Inc., Walnut Creek, CA, USA). Results were expressed as the relative percentage of each individual FA present in the sample.

2.4. Electrode preparation

The steel used in this study is a carbon steel with a chemical composition 0.077 wt. % Cr; 0.230 wt. % Si; 0.011 wt. % Ti; 0.680 wt. % Mn; 0.370 wt. % C; 0.016 wt. % S; 0.059 wt. % Ni; 0.160 wt. % Cu; 0.009 wt. % Co and the remainder iron (Fe). The working surface was subsequently ground with 180 and 1200 grit grinding papers, cleaned by distilled water and ethanol.

2.5. Preparation of solutions

The aggressive solutions of 1 M HCl were prepared by dilution of analytical grade 37% HCl with distilled water. Inhibitor was dissolved in acid solution at the required concentrations (3g/L), and the solution in the absence of inhibitor was taken as blank for comparison purposes. The test solutions were freshly prepared before each experiment by adding extract of *SMO* directly to the corrosive solution. Concentrations of *Silybum Marianum* oil (SMO) are 1.2, 1.8, 2.4 and 3 g/L.

2.5. Electrochemical tests

2.5.1. Electrochemical impedance spectroscopy

The electrochemical measurements were carried out using Volta lab (Tacussel Radiometer PGZ 100) potentiostat and controlled by Tacussel corrosion analysis software model (Volta master 4) at under static condition. The corrosion cell used had three electrodes. The reference electrode was a saturated calomel electrode (SCE). A platinum electrode was used as auxiliary electrode of surface area of 1 cm^2. The working electrode was carbon steel. All potentials given in this study were referred to this reference electrode. The working electrode was immersed in test solution for 30 minutes to a establish steady state open circuit potential (E_{ocp}). After measuring

the E_{ocp}, the electrochemical measurements were performed. All electrochemical tests have been performed in aerated solutions at 303 K. The electrochemical impedance spectroscopy experiments were conducted in the frequency range between 100 kHz and 10 mHz, after 30 min of immersion in solution tested.
The inhibition efficiency of the inhibitor was calculated from the charge transfer resistance values using the following equation [16]:

$$\eta_z\% = \frac{R_{ct}^{i} - R_{ct}^{\circ}}{R_{ct}^{i}} \times 100 \quad (1)$$

Where, R°_{ct} and R^{i}_{ct} are the charge transfer resistance in absence and in presence of inhibitor, respectively.

2.5.2. Potentiodynamic polarization
The electrochemical behavior of carbon steel sample in inhibited and uninhibited solution was studied by recording anodic and cathodic potentiodynamic polarization curves. Measurements were performed in the 1M HCl solution containing different concentrations of the tested inhibitor by changing the electrode potential automatically from -800 to -300 mV versus corrosion potential at a scan rate of 1 $mV.s^{-1}$. The linear Tafel segments of anodic and cathodic curves were extrapolated to corrosion potential to obtain corrosion current densities (I_{corr}).
The inhibition efficiency was evaluated from the measured I_{corr} values using the relationship [17]:

$$\eta_{\text{Tafel}}(\%) = \frac{I_{corr} - I_{corr(i)}}{I_{corr}} \times 100 \quad (2)$$

where I_{corr} and $I_{corr(i)}$ are the corrosion current densities for steel electrode in the uninhibited and inhibited solutions, respectively.

2.6. Scanning electron microscopy (SEM)
The morphology of state surface was performed using a JEOL JSM-5800 Scanning Electron Microscopy. The energy of the acceleration beam employed was 20 kV. The analysis by SEM was carried out on the surface of carbon steel samples before and after immersion in the acidic solutions with and without the optimal concentration of *Silybum Marianum* oil (SMO).

3. Results and discussion

3.1. Silybum marianum oil analysis

Silybum marianum (*SM*) seeds afforded 19% of oil after hexane extraction, this yields are lower than that reported for *SM* seeds cultivated in Pakistan (26%) [18].
Table 1 lists the fatty acid composition of *SM* oil. The main fatty acids of *SM* oil were linoleic, oleic, palmitic and Stearic acid, which comprised approximately 99.7% of the total fatty acids. Linoleic acid is indispensable for the healthy growth of human skin. It can be transformed by the organism into series of long fatty acids chains, which are the precursors of eicosanoids [19]. Dietary fat rich in linoleic acid, apart from preventing cardiovascular disorders, such as coronary heart diseases and atherosclerosis, also prevents high blood pressure [20]. Among the many fatty acids, the linoleic acid content was the highest, 48.26%. This linoleic acid content was higher than that of other Moroccan oil like argan oil (34%), olive oil (13.2%) and sesame oil (42.1%) [21-22], but lower than linoleic acid content in cactus oil (62.3%) and nigella oil (58.5%) [23-24].
Among the monounsaturated fatty acids, the oleic acid content was the second highest, 27.71%, comprising approximately 93.5% of monounsaturated fatty acid content. The total unsaturated fatty acid content was 78.11%, in which the monounsaturated and polyunsaturated fatty acids comprised 29.63 and 48.48% of the total fatty acids, respectively. The total saturated fatty acid of *S. marianum* oil is 21.67%, which makes it strongly resistant to oxidative rancidity. Among the saturated fatty acids of *SM* oil, palmitic and Stearic acid were the highest, 7.67 and 4.97%, respectively.

Table 1: Fatty acid composition of *Silybum marianum* oil.

Fatty acid	% of total fattyacids	Fatty acid	% of total fattyacids
Myristic C 14: 0	0.07	Linolenic C 18 :3	0.22
Palmitic C 16: 0	7.67	Arachidic C 20 :0	3.99
Palmitoleic C 16:1	0.05	Eicosenoic C 20 :1	1.11
Margaric C 17:0	0.07	BehenicC22 :0	3.85
Stearic C 18:0	4.97	LignocericC24 :0	1.05
Oleic C 18:1Δ9	27.71	MUFA	29.63
C 18: 1 Δ11	0.76	PUFA	48.48
Linoleic C 18 :2	48.26	SFA	21.67

SFA: saturated fatty acids, MUFA: monounsaturated fatty Acids. PUFA: Polyunsaturated fatty acids.

3.2. Polarization curves

Potentiodynamic polarization curves have been recorded for carbon steel in 1 M HCl solution in different concentrations of SMO at 303 K (Fig. 1). Electrochemical parameters extracted from polarization curves including corrosion potential (E_{corr}), corrosion current density (I_{corr}), cathodic Tafel slopes (β_c) and anodic Tafel slopes (β_a) have been measured by Tafel extrapolation and presented in Table 2.

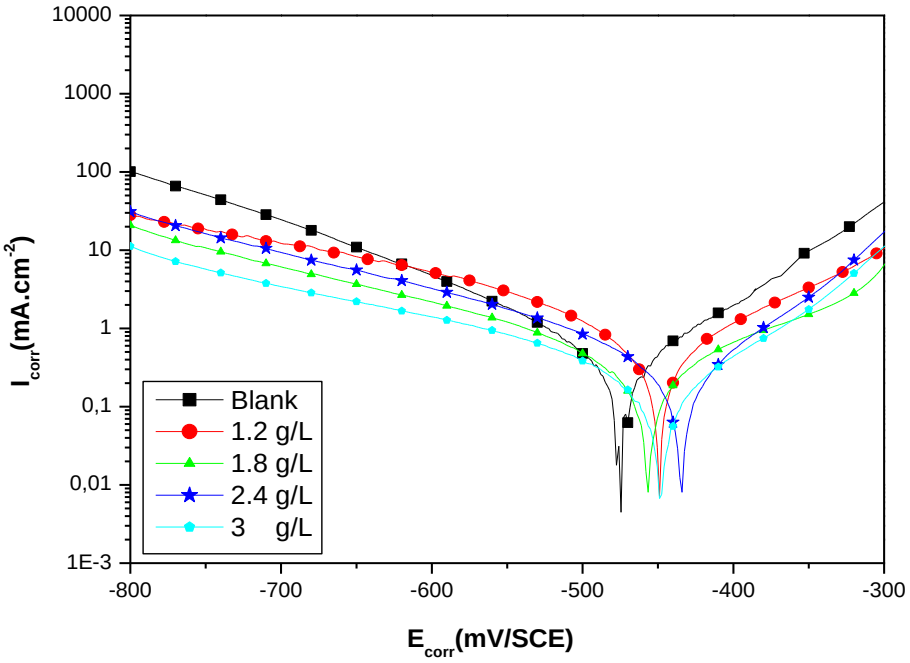

Figure 1: Potentiodynamic polarization curves for carbon steel in 1 M HCl at various concentrations of *SM* oil at 303 K

It can be seen from Fig. 1 that the existence of inhibitor molecule in the corrosive medium increases anodic and cathodic over potentials, and decreases corrosion current (I_{corr}). These changes increase with increasing inhibitor concentration. This behavior supports the adsorption of inhibitor onto metal surface and causes a barrier effect for mass and charge transfer for anodic and cathodic reactions. The cathodic potential diagrams (Fig. 1), which give rise to parallel lines, show that increasing concentrations of SMO do not change the cathodic reduction reaction mechanism of hydrogen. Thus, the mechanisms of hydrogen evolution and the reduction of H^+ ions at the carbon steel surface occur mainly through a charge transfer mechanism. The cathodic Tafel slope (β_c) show slight

changes with the addition of SMO, which suggests that the inhibiting action occurred by simple blocking of the available cathodic sites on the metal surface, which lead to a decrease in the exposed area necessary for hydrogen evolution.

Table 2: Potentiodynamic polarization parameters for carbon steel in1 M HCl at various concentrations of SM oil at 303 K.

Medium	*Conc (g/L)*	*$-E_{corr}$ (mV_{SCE})*	*β_a (mV/dec)*	*$-\beta_c$ (mV/dec)*	*I_{corr} ($\mu A\ cm^{-2}$)*	*η_{Tafel} (%)*	*θ*
1 M HCl	—	491	101	138	579	—	—
SMO	1.2	449	74	90	280	51.6	0.516
	1.8	457	98	109	181	68.7	0.687
	2.4	449	60	78	135	76.7	0.767
	3.0	473	75	76	63	89.1	0.891

There is no definite trend observed in the E_{corr} values in the presence of SMO. In literature [25], it has been reported that (i) if the displacement in E_{corr} is > 85 mV with respect to E_{corr}, the inhibitor can be seen as a cathodic or anodic type and (ii) if displacement in E_{corr} is < 85, the inhibitor can be seen as mixed type. In the present study, shift in E_{corr} values is in the range of 18-42 mV, suggesting that SMO acted as mixed type of inhibitor [26].

3.3. Electrochemical impedance spectroscopy measurements

The corrosion behaviour of carbon steel in 1 M HCl solution in the presence of SMO was investigated by EIS at 303 K after 30 min of immersion. Fig. 2 shows the results of EIS experiments in the Nyquist representation. After analyzing the shape of the Nyquist plots, it is concluded that the curves approximated by a single capacitive semi-circles, showing that the corrosion process was mainly charge transfer controlled [27]. The general shape of the curves is very similar for all samples; the shape is maintained throughout the whole concentrations, indicating that almost no change in the corrosion mechanism occurred due to the inhibitor addition [27]. The diameter of Nyquist plots (R_{ct}) increases on increasing the SMO concentration. These results suggest the inhibition behaviour of SMO on corrosion of carbon steel in 1 M HCl solution.

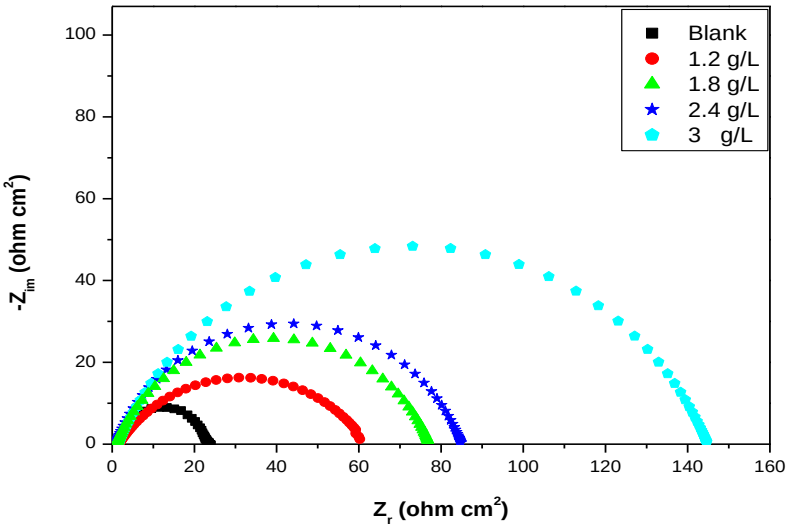

Figure 2: Nyquist diagrams for carbon steel in 1 M HCl containing different concentrations of SMO at 303 K.

Table 3 summaries the impedance data from EIS experiments performed in the absence and presence of increasing SMO concentration.

Table 3: Impedance parameters for corrosion of carbone steel in 1M HCl at various contents of SM oil.

Medium	*Conc (g/L)*	R_{ct} *(Ω cm²)*	f_{max} *(Hz)*	C_{dl} *(µF cm⁻²)*	η_z *(%)*
1 M HCl	—	20	63	126	—
SMO	1.2	57	25	112	64.9
	1.8	81	20	98	75.3
	2.4	84	25	76	76.2
	3.0	175	40	23	88.6

The double-layer capacitance (C_{dl}) was calculated from the following equation:

$$C_{dl} = \frac{1}{2\pi f_{max} R_{ct}} \qquad (3)$$

where f_{max} is the frequency at which the imaginary component of the impedance is maximal.
Charge-transfer resistance increases from 20 to 175 Ω cm^2 and double layer capacitance C_{dl} decreases from 126 to 23 µF/cm^2 with the increase of SMO concentration. The decrease in C_{dl} means that the adsorption of inhibitor takes place on the carbon steel surface in acidic solution. The increase in the charge-transfer resistance leads to an increase of inhibition efficiency. The results indicate good agreement between the values of corrosion efficiency as obtained from the polarization measurements and impedance technique. It is concluded that the corrosion rate depends on the chemical nature of the electrolyte rather than the applied technique [28].

3.4. Effect of temperature

The effect of temperature on the inhibition performance of *SM* oil for carbon steel in 1 M HCl solution in the absence and presence of 3g/L concentration at temperature ranging from 303 to 333 K was obtained by potentio-dynamic polarization measurements (Figs 3 and 4). The results are given in Table 4.

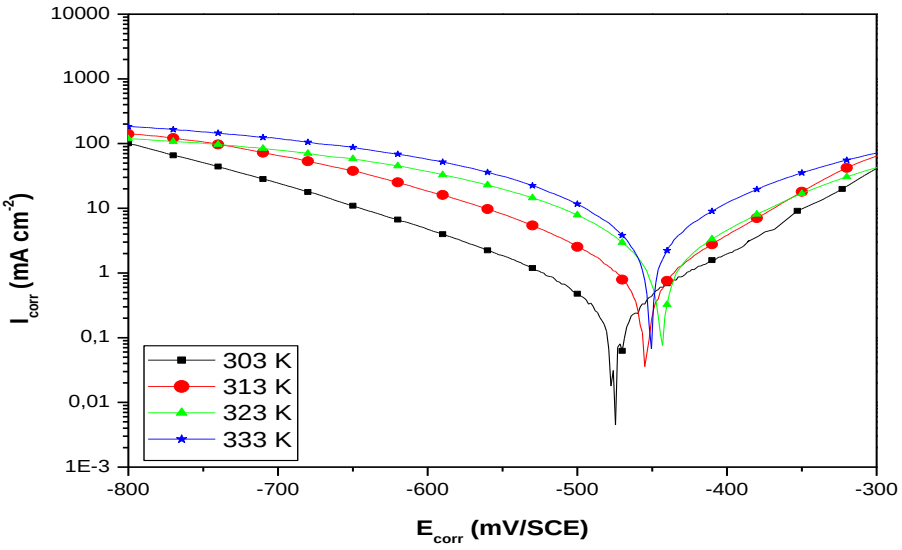

Figure 3: Potentiodynamic polarisation curves of carbon steel in 1 M HCl at different temperatures.

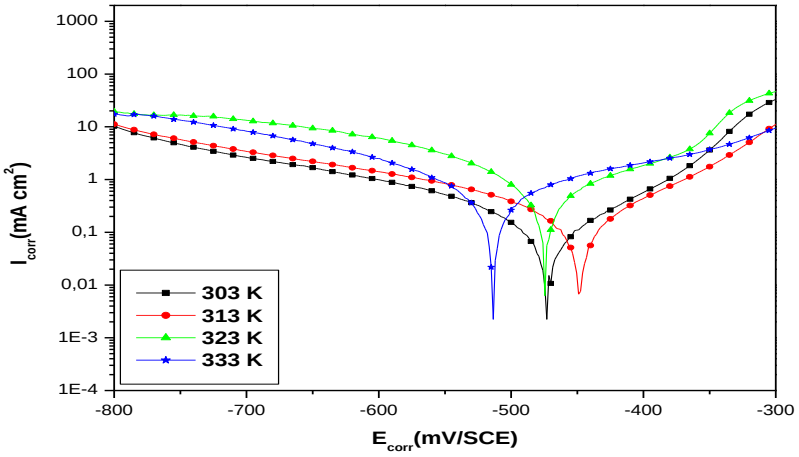

Figure 4: Potentiodynamic polarisation curves of carbon steel in 1M HCl in the presence of the optimum concentration of SMO at different temperatures.

The inhibition efficiencies are found to decrease with increasing the temperature from 303 K to 333 K. This behavior can be interpreted that the increase in temperature results in desorption of the inhibitor molecules from the surface of carbon steel.
Table 4 shows that the corrosion current density (I_{corr}) increased more rapidly with increasing temperature both in uninhibited and inhibited solutions. These results confirm that SMO acts as an efficient inhibitor for carbon steel in 1 M HCl in the range of temperature studied.

Table 4: Various corrosion parameters for carbon steel in 1 M HCl in absence and presence of optimum concentration of SMO at different temperatures.

Medium	*Temp (K)*	*-E_{corr} (mV_{SCE})*	*I_{corr} ($\mu A\ cm^{-2}$)*	*-β_c (mV/dec)*	*η_{Tafel} (%)*
Blank	303	475	579	138	—
	313	448	781	57	—
	323	457	882	107	—
	333	477	999	161	—
SMO	303	473	63	75	89.1
	313	452	121	131	84.5
	323	477	258	86	70.7
	333	516	336	106	66.4

The dependence of the corrosion rate on temperature can be expressed by the Arrhenius equation [29]:

$$I_{corr} = k \exp\left(-\frac{E_a}{RT}\right) \qquad (4)$$

Where E_a is the apparent activation corrosion energy, R is the universal gas constant and k is the Arrhenius pre-exponential constant Arrhenius plots for the corrosion density of carbon steel in the case of SMO are given in Fig.5. Values of apparent activation energy of corrosion (E_a) for carbon steel in 1 M HCl with the absence and presence of SMO were determined from the slope of Ln (I_{corr}) versus 1/T plots and shown in Table 5.

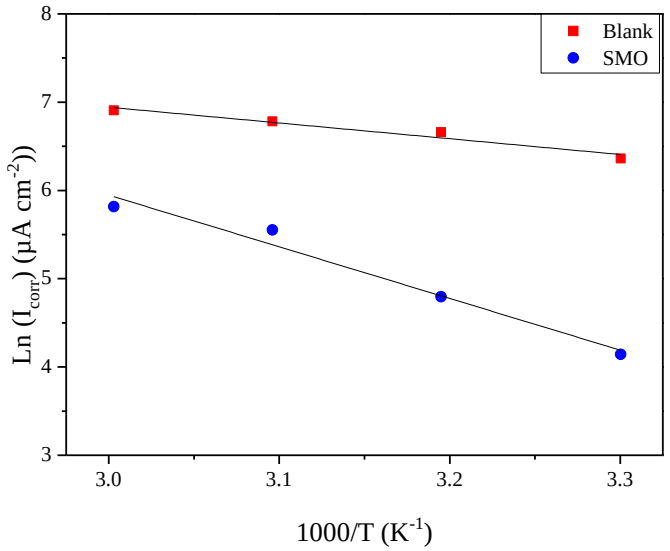

Figure 5: Arrhenius plots of carbon steel in 1 M HCl with and without 3 g/L of SMO.

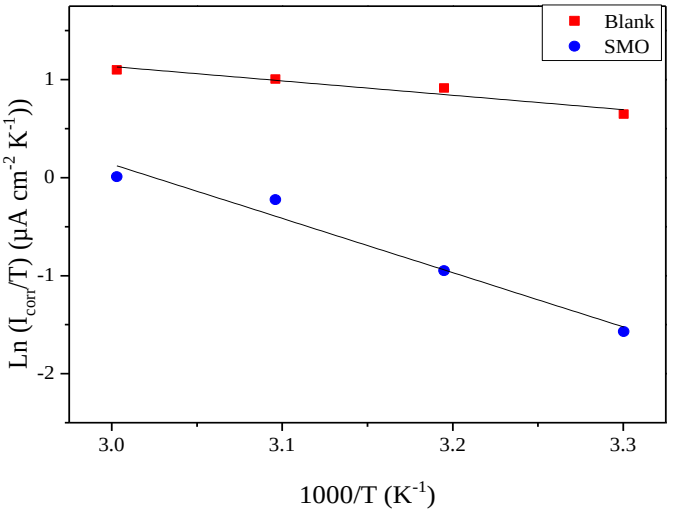

Figure 6: Transition Arrhenius plots of carbon steel in 1 M HCl with and without 3 g/L of SMO.

Table 5: The values of activation parameters E_a, ΔH_a and ΔS_a for carbon steel in 1 M HCl in the absence and presence of 3 g/L of SMO.

Medium	E_a *(kJ/mol)*	ΔH_a *(kJ/mol)*	ΔS_a *(J/mol K)*
Blank	16.21	13.64	-204.48
SMO	49.33	47.04	-112.58

According to the report in literature [30], higher value of E_a was considered as physiadsorption that occurred in the first stage. Because the electrochemical corrosion is relevant to heterogeneous reactions, the preexponential factor k in the Arrhenius equation is related to the number of active centers. There are two possibilities about these active centers with different E_a on the metal surface: (1) the activation energy in the presence of inhibitors is

lower than that of pure acidic medium, namely E_a(-inh) < E_a(HCl), which suggests a smaller number of more active sites remain uncovered in the corrosion process; (2) the activation energy in the presence of inhibitor is higher than that of pure acidic medium, E_a(inh) > E_a(HCl), which represents the inhibitor adsorbed on most active adsorption sites (having the lowest energy) and the corrosion takes place chiefly on the active sites (having higher energy).

The data in Table 5 specifically indicate that the value of E_a in the presence of SMO is larger than that in the absence of SMO. Thus, it is clear that the adsorption of SMO on carbon steel surface blocks the active sites from acid solution and consequently increases the apparent activation energy. Then, it can be suggested that the SMO adsorb by physisorption on metallic surface.

Activation parameters like enthalpy (ΔH_a) and entropy (ΔS_a) for the dissolution of carbon steel in 1 M HCl in the absence and presence of 3 g/L of SMO were calculated from the transition state equation (Eq. (5)) [31]:

$$I_{corr} = \frac{RT}{Nh}\exp\left(\frac{\Delta S_a}{R}\right)\exp\left(-\frac{\Delta H_a}{RT}\right) \quad (5)$$

where I_{corr} is the corrosion rate, A is the pre-exponential factor, h is Planck's constant, N is the Avogadro number, R is the universal gas constant, ΔH_a is the enthalpy of activation and ΔS_a is the entropy of activation.

Fig. 6 showed the Arrhenius plots of Ln (I_{corr}/T) versus 1/T gave straight lines with slope ($-\Delta H_a/R$) and intercept (Ln R/Nh + ΔS_a/R) from which ΔH_a and ΔS_a values were calculated. The activation parameters are given in Table 5.

The positive sign of the enthalpies ΔH_a reflects the endothermic nature of the steel dissolution process whereas large negative values of entropies ΔS_a from SMO imply that the activated complex in the rate determining step represents an association rather than a dissociation step, meaning that a decrease in disordering takes place on going from reactants to the activated complex [32,33].

3.5. Isotherme adsorption

The mechanism of the interaction between inhibitor and the electrode surface can be explained using adsorption isotherms. The fractional surface coverage θ for different concentrations of SM oil in 1 M HCl solution can be easily determined using the flowing formula are:

$$\theta = \frac{I_{corr} - I_{corr(i)}}{I_{corr}} \quad (6)$$

As it is known that adsorption of an organic adsorbate onto metal-solution interface can be presented as a substitution adsorption process between the organic molecules in the aqueous solution $Org_{(sol)}$ and the water molecules on the metallic surface $H_2O_{(ads)}$:

$Org_{(sol)} + n\,H_2O_{(ads)} \leftrightarrow Org_{(ads)} + n\,H_2O_{(sol)}$

Where $Org_{(sol)}$ and $Org_{(ads)}$ are the organic molecules in the aqueous solution and adsorbed on the metallic surface, respectively, $H_2O_{(ads)}$ is the water molecules on the metallic surface, n is the size ratio representing the number of water molecules replaced by one molecule of organic adsorbate.

In order to evaluate the adsorption process of SMO carbon steel surface, Langmuir, Temkin and Frumkin adsorption isotherms were obtained according to the following equations:

Langmuir : $$\frac{C_{inh}}{\theta} = \frac{1}{K} + C_{inh} \quad (7)$$

Frumkin : $$\frac{\theta}{1-\theta}\exp\left(-2a\theta\right) = KC_{inh} \quad (8)$$

Temkin : $$\exp\left(-2a\theta\right) = KC_{inh} \quad (9)$$

Where θ is the surface coverage of the metal surface, K the adsorption-desorption equilibrium constant, C_{inh} the inhibitor concentration and a is the lateral interaction term describing the molecular interactions in the adsorption layer and the heterogeneity of the surface. The fractional coverage values θ as a function of inhibitor concentration can be obtained from potentiodynamic polarization.

To determine which adsorption isotherm best fits the surface's coverage, the respective plots were obtained in Figs. 7-9. These curves represent adsorption isotherms that are characterized by, in a first part, a sharp rising, followed by another part, a gradual rising (less significant than in the first part), indicating formation of an adsorbed molecules layer on the steel surface. By far, the best fit was obtained with the Temkin isotherm (strong correlation R^2 = 0.98365). The plots of C_{inh}/θ vs. C_{inh} yield a straight line (Fig. 7). This confirms that the inhibitor obeys Temkin adsorption isotherm at 1 M HCl medium.

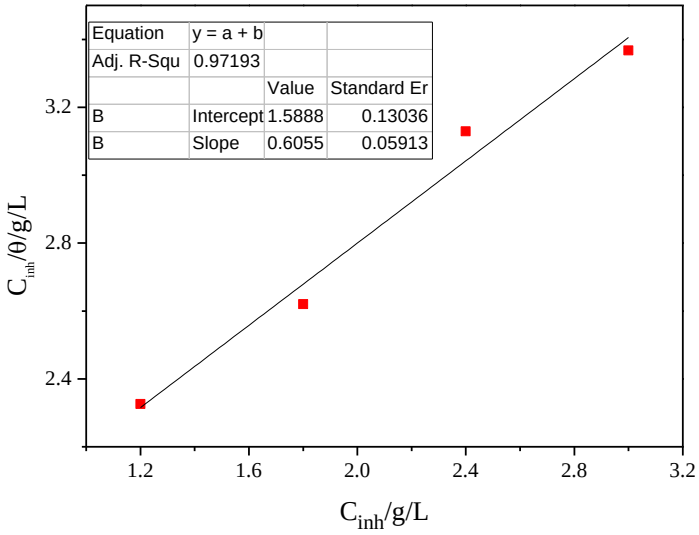

Figure 7: Langmuir adsorption plots obtained for carbon steel in 1 M HCl containing different concentrations of SMO.

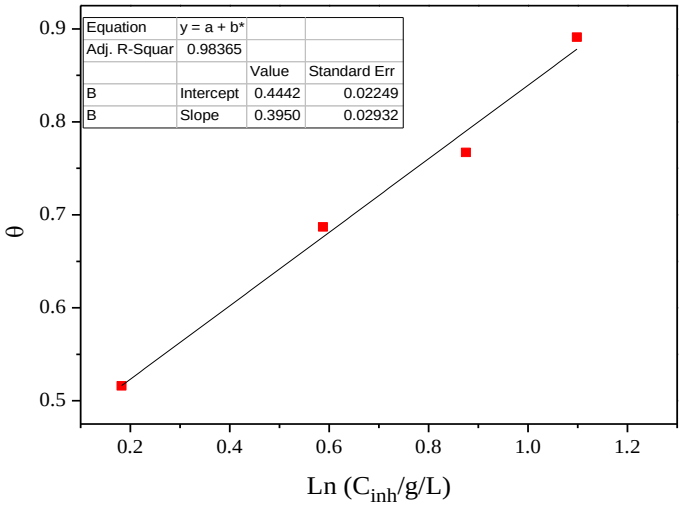

1

Figure 8: Temkin adsorption plots obtained for carbon steel in 1 M HCl containing different concentrations of SMO.

It is very important to note that discussion of the adsorption isotherm behavior, using natural product extracts as inhibitors, in terms of the standard free energy of adsorption value, is not possible because the molecular mass of the extract components is not known. Some authors [34-36], in their study on acid corrosion with plant extracts and essential oils, noted the same limitation.

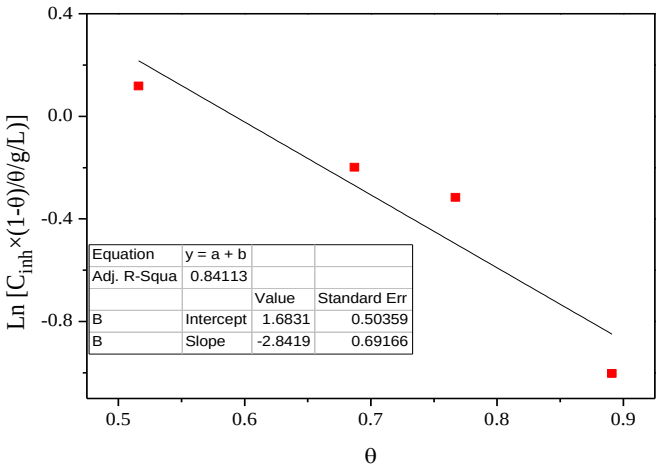

Figure 9: Frumkin adsorption plots obtained for carbon steel in 1 M HCl at different concentrations of SMO.

3.6. Scanning electron microscopy (SEM)

The SEM images were recorded in order to confirm the protective film formation during the corrosion process. Fig. 10A signifies the SEM image of the polished carbon steel surface and except the presence of polishing scratches; the surface shows the absence of noticeable defects such as pits and cracks. The SEM image of the carbon steel surface after 6 h immersion in 1 M HCl is shown in Fig. 10B. It exposes that the surface was rough and harshly corroded for the reason that of the violent attack by 1 M HCl. Fig. 10C illustrate SEM images of the carbon steel specimens for the same period of immersion time in 1 M HCl solution containing 3 g/L of SM oil. Figure reveal the formation of a protective film of the inhibitor on the carbon steel surface which inhibits the corrosion considerably in acidic medium.

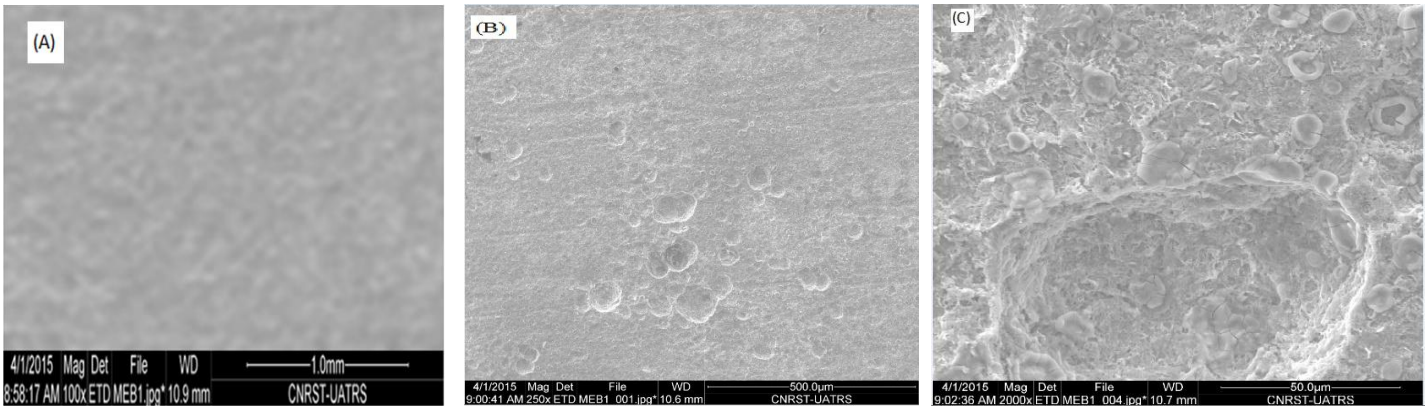

Figure 10: SEM images: (A) only surface polishing, (B) after immersion in 1 M HCl without SMO, (C) after immersion in 1 M HCl in presence of 3 g/L of SMO.

Conclusions

The *Silybum Marianum* oil (SMO) is an efficient inhibitor for carbon steel in 1 M HCl. The inhibition efficiency increases with the addition of inhibitor and reached a maximum of 89.1 % in the presence of 3 g/L of inhibitor. The inhibition efficiency decreases with the increase in temperature. The adsorption of SMO on carbon steel obeys Temkin adsorption isotherm. Polarization studies show that the inhibitor as a mixed type inhibitor. The electrochemical impedance spectroscopy and SEM confirms the formation of protective film on the carbon steel surface. The inhibition efficiencies determined by EIS and PDP methods are in good agreement.

References

1. Zhang Q. B., Hua Y. X., *Electrochim. Acta* 54 (2009) 1881.
2. Fouda A.S., Shalabi K., Ezzat R. *J. Mater. Environ. Sci.* 6 (4) (2015) 1022-1039.
3. Quraishi M. A., ardar R. S., *Mater. Chem. Phys*. 78 (2003) 425
4. Obot B., Obi-Egbedi N.O., *Corros. Sci*. 52 (2010) 198 –204.
5. El-Hajjaji F., Zerga B., Sfaira M., Taleb M., Ebn Touhami M., Hammouti B., Al-Deyab S.S., Benzeid H., Essassi E.M., *J. Mater. Environ. Sci.* 5 (2014) 255-262
6. Hari Kumar S., Karthikeyan S., *J. Mater. Environ. Sci.* 4 (5) (2013) 675-984
7. ElHajjaji F., Greche H., Taleb M., Chetouani A., Aouniti A., Hammouti B., *J. Mater. Environ. Sci.* 7 (2016) 566-578
8. Yadav M., Sinha R.R., Kumar S., Bahadur I., Ebenso E.E., *J. Mol. Liq*. 208 (2015) 322 –332.
9. Kharbach Y., Haoudi A., Skalli M.K., Kandri Rodi Y., Aouniti A., Hammouti B., Senhaji O., Zarrouk A. *J. Mater. Environ. Sci.* 6 (10) (2015) 2906-2916
10. Vashisht H., Kumar S., Bahadur I., Singh G., *Int. J. Electrochem. Sci*. 8 (2013) 684 – 699.
11. El Bribri A., Tabyaoui M., Tabyaoui B., El Attari H., Bentiss F., *Mater. Chem. Phys* 141 (2013) 240-247.
12. AL-Senani G M., AL-Saeedi S I.., AL-Mufarij R S. *J Mater. Environ. Sci.* 7 (7) (2016) 2240-2251
13. Boumhara K., Tabyaoui M., Jama C., Bentiss F., *J. Ind. Eng. Chem* 29 (2015) 146–155.
14. ISO 659:2009, (2009) Oilseeds- Determination of oil content (Reference method).
15. ISO 5508. (1990). Animal and vegetable fats and oils - Analysis by GC of methyl esters of fatty acids.
16. Zarrok H., Zarrouk A., Hammouti B., Salghi R., Jama C., Bentiss F., *Corros. Sci*. 64 (2012) 243.
17. Gece G., Bilgic S., *Corros. Sci*. 52 (2010) 3435–3443.
18. Khan I., Khattak H.U., Ullah I., Bangash F.K,. (2007) *Jour. Chem. Soc. Pak*, 29:6, 545-548
19. Nasri N., Khaldi A., Fady B., Triki S., *Phytochem*., 66, 1729(2005).
20. Vles R. O., Gottenbos J. J., New York, USA, McGraw Hill (1989).
21. Gharby S., Harhar H., El Monfalouti H., Kartah B., Maata N., Guillaume D., Charrouf Z., *Med. J. Nutr.Metab*,(2012) 5:31–38.
22. Gharby S., Harhar H., Bouzoubaa Z., Asdadi A., El Yadini A.,Charrouf Z., *J. Saudi. Soc. Agri. Sci* (2015), (in press) http://dx.doi.org/10.1016/j.jssas.2015.03.004
23. Taoufik F., Zine S., El Hadek M., Idrissi Hassani L.M., Gharby S., Harhar H., Matthaus B., *Medi. J.Nutr. Metab*, (2015). 8:2, 85-92,
24. Gharby S, Harhar H., Guillaume D., Roudani A., Boulbaroud S., Ibrahimi M., Ahmad M., Sultana S., Ben Hadda T., Chafchaouni-Moussaoui I.,Charrouf Z., *J. Saudi. Soc. Agri. Sci*.(2015) 14, 172–177.
25. Ferreira E.S., Giancomelli C., Giacomelli F.C., Spinelli A., *Mater. Chem. Phys*. 83 (2004) 129.
26. Riggs O.L., Jr. Corrosion Inhibitors, 2nd ed.; C. C. Nathan: Houston, TX, USA, 1973; p 109.
27. Rosliza R., Wan Nik W.B., Senin H.B., *Mater. Chem. Phys*. 107 (2008) 281.
28. Abdel-Gaber M., Abd-El-Nabey B.A., Sidahmed I.M., El-Zayaday A.M., Saadawy M., *Corros. Sci* 48 (2006) 2765.
29. Solmaz R., Kardas G., Ulha M.C., Yazıcı B., Erbil M., *Electrochim. Acta.,* 53 (2008), 5941.
30. Chen W., Luo H.Q., Li N.B., *Corros. Sci*. 53 (2011) 3356.
31. Abd El-Rehim S.S., Ibrahim M.A.M., Khaled K.F., *J. Appl. Electrochem*., 29 (1999) 593.
32. Martinez S., Stern I., *Appl. Surf. Sci*. 199 (2002) 83.
33. Dahmani M., Et-Touhami A., Al-Deyab S.S., Hammouti B., Bouyanzer A., *Int. J. Electrochem. Sci*. 5 (2010) 1060.
34. Bobina M., Kellenberger A., Millet J.P., Muntean C., Vaszilcsin N., *Corros. Sci*. 69 (2013) 389.
35. Gunasekaran G., Chauhan L.R., *Electrochim. Acta* 2004, 49, 4387.
36. X. Li, S. Deng, H. Fu, *Corros. Sci*. 62 (2012) 163.